Direct Monocular Odometry Using Points and Lines

Shichao Yang, Sebastian Scherer

***Abstract*— Most visual odometry algorithm for a monocular camera focuses on points, either by feature matching, or direct alignment of pixel intensity, while ignoring a common but important geometry entity: edges. In this paper, we propose an odometry algorithm that combines points and edges to benefit from the advantages of both direct and feature based methods. It works better in texture-less environments and is also more robust to lighting changes and fast motion by increasing the convergence basin. We maintain a depth map for the keyframe then in the tracking part, the camera pose is recovered by minimizing both the photometric error and geometric error to the matched edge in a probabilistic framework. In the mapping part, edge is used to speed up and increase stereo matching accuracy. On various public datasets, our algorithm achieves better or comparable performance than state-of-the-art monocular odometry methods. In some challenging texture-less environments, our algorithm reduces the state estimation error over 50%.**

I. Introduction

Visual odometry (VO) and Simultaneous localization and mapping (SLAM) have become popular topics in recent years due to their wide application in robot navigation, 3D reconstruction, and virtual reality. Different sensors can be used such as RGB-D cameras [1], stereo cameras [2] and lasers, which could provide depth information for each frame, making it easier for state estimation and mapping. However for some applications such as weight constrained micro aerial vehicles [3], monocular cameras are more widely used due to their small size and low cost. Therefore, in this work, we are aiming at the more challenging monocular VO.

There are typically two categories of VO and vSLAM approaches: (1) feature based methods such as PTAM [4] and ORB SLAM [5]. They rely on feature point extraction and matching to create sparse 3D map used for pose estimation by minimizing re-projection geometric error. (2) Recently, direct method [6] [7] also becomes popular. It directly operates on the raw pixel intensity by minimizing photometric error without feature extraction. These two methods both have their advantages. Reprojection geometric error of keypoints is typically more robust to image noise and large geometric distortions and movement. Direct method on the other hand, exploits much more image information and can create dense or semi-dense maps.

In this paper, we utilize points and edges to combine the advantages of the above two approaches. Edge is another important feature apart from points. It has been used for stereo [8] and RGB-D VO [9], but receives less attention in monocular VO. The detection of edges is less sensitive to lighting changes by nature. For example, in a homogeneous environment of Fig. 1, direct method using points only may not work robustly due to small image gradient, but we can still detect many edges shown in blue in the figure which could be used for state estimation and mapping. In our system, we maintain a semi-depth map for the keyframe's high gradient pixels as in many direct VO methods [6]. We also detect and match edges for each frame. Then in the tracking part, we jointly optimize both photometric error and geometric error to the corresponding edge if it has. In the mapping part, edges could also be used to guide and speed up the stereo search and also improve depth map quality by edge regularizing. By doing this, the proposed VO can increase the accuracy of state estimation and also create a good semi-dense map. We demonstrate this through various experiments.

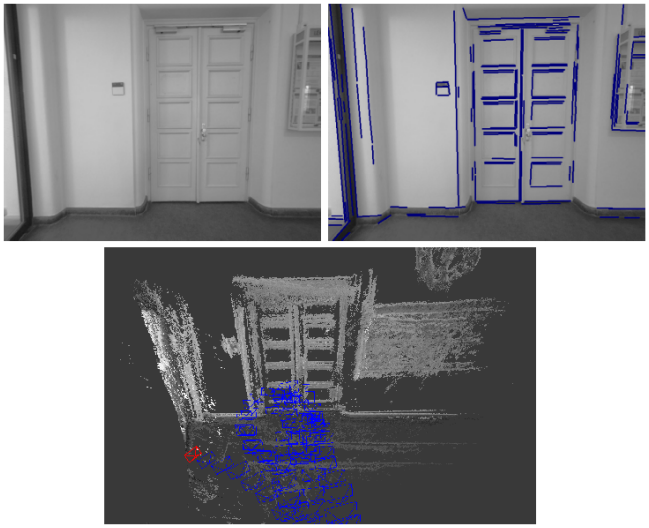

Fig. 1. Tracking and 3D reconstruction on TUM mono dataset using our edge based visual odometry. The top image shows the homogeneous wall surface with low image gradients, which is challenging for VO only minimizing photometric error. However, edge shown in blue can still be detected to improve the tracking and mapping performance.

In summary, our main contributions are:

- A real-time monocular visual odometry algorithm incorporating points and edges, especially suitable for texture-less environments.
- Provide an uncertainty analysis and probabilistic fusion of points and lines in tracking and mapping.
- Develop analytical edge based regularization
- Outperform or comparable to existing direct VO in many datasets.

In the following section, we discuss related work. In

The Robotics Institute, Carnegie Mellon University, 5000 Forbes Ave, Pittsburgh, PA 15213, USA. {shichaoy, basti}@andrew.cmu.edu

Section III, we provide the problem formulation. Tracking and mapping using points and edges are presented in Section IV and Section V respectively, which also include probabilistic uncertainty analysis of different observation model. In Section VI, we provide experimental comparison with the state-of-art algorithm. Finally, conclusion and future work is discussed in Section VII

II. Related Work

Our algorithm utilizes edges to combine feature based and direct VO. We briefly introduce these three aspects.

A. Feature based VO

There have been many feature point based VO and SLAM, for example LibVISO [2] and ORB SLAM [5]. They first extract image features then track or match them across images. The camera pose is estimated by solving the PnP (Perspective N-Point Projection) problem to minimize geometric error which is more robust to image noise and has a large convergence basin [5] [10]. The drawback is that the created map is usually sparse. A separate direct mapping algorithm is required to get a semi-dense map [11].

B. Direct VO

In recent years, direct method [12] also becomes popular. It optimizes the geometry directly on the image intensities without any feature extraction so it can work in some textureless environments with few keypoints. It has been used for real-time application of different sensors for example DVO for RGB-D cameras [13] and LSD SLAM for monocular cameras [7]. The core idea is to maintain a semi-dense map for keyframes then minimize the photometric error which is a highly non-convex function thus it requires good initial guess for the optimization. In between direct and feature based methods, SVO combines direct alignment and feature points and can be used for high frame rate cameras.

C. Edge based VO

Edges are another important feature apart from points especially in man-made environments. Edges are more robust to lighting changes and preserve more information compared to single points. Line-based bundle adjustment has been used in SLAM or SfM [14] [15] which are computationally expensive and require at least three frames for effective optimization. Line-based VO without bundle adjustment has recently been used for stereo cameras [16] [8] and RGB-D [17] [9] and monocular cameras [18] [19]. Kuse *et al.* minimize the geometric error to its nearby edges pixels through distance transform [9] which might cause wrong matching due to false detected edges and broken edges while our line segment matching could greatly reduce the error. Some works only minimize geometric error of two edge endpoints [8] [17] which may generate large error for monocular cameras due to inaccurate depth estimation.

III. Problem Description

A. System Overview

Our algorithm is a frame to keyframe monocular VO. We maintain a semi-depth map for the high gradient pixels in the keyframe. Then for each incoming new frame, there are three steps. First, detect line segments and match them with the keyframe's edges. The second step is camera pose tracking. We minimize a combination of pixel photometric error and geometric reprojection error if the pixel belongs to an edge. Lastly, we update the depth map through variable baseline stereo. Edges are used to speed up the stereo search for those edge pixels and also improve reconstruction through an efficient 3D line regularization.

B. Notations

We denote an intensity image as $I : \Omega \subset \mathbb{R}^2 \mapsto \mathbb{R}$, where Ω represents the image domain. We keep a per-pixel inverse depth map for a reference keyframe $D : \Omega \subset \mathbb{R}^2 \mapsto \mathbb{R}^+$ and inverse depth variance $V : \Omega \mapsto \mathbb{R}^+$.

The camera projection function is defined as $\pi : \mathbb{R}^3 \mapsto \mathbb{R}^2$, which projects a camera-centered 3D point onto image plane. The inverse projection function is then $\pi^{-1} : (\mathbb{R}^2, \mathbb{R}) \mapsto \mathbb{R}^3$ which back-projects an image pixel to the 3D space given its depth.

The transformation between the current frame and reference keyframe is defined by a rigid transformation $T \in SE(3)$. For an efficient optimization of T, we use the minimal manifold representation by elements of the Lie-algebra $\xi \in \mathfrak{se}(3)$ [20], which is expressed by twist $\xi = (\mathbf{t}; \mathbf{w})^T \in \mathbb{R}^6$. $\mathbf{t} \in \mathbb{R}^3$ is the translation component and $\mathbf{w} \in \mathbb{R}^3$ is the rotation component, which can form rotation matrix by the corresponding exponential map: $R(\mathbf{w}) = \exp([\mathbf{w}]_\times) \in SO(3)$.

A warping function is defined as $\tau : \Omega_1 \times \mathbb{R} \times \mathbb{R}^6 \mapsto \Omega_2$. It takes the parameters of a pixel $x \in \Omega_1$ in the first image I_1, its depth d and relative camera transformation ξ, then returns the re-projection point in second image I_2. Internally, it first back-projects x to 3D point by π^{-1}, transforms it using ξ, then projects to another frame using π.

An edge is represented by L in 3D space and l in 2D image plane. All the edge pixels in an image are defined as $M : \mathbb{R}^2 \mapsto l$ which maps a pixel to its edge. Most of the edge pixels M belong to the high gradient pixel set Ω.

IV. Tracking

A. Overview

In the tracking thread, the depth map D_{ref} of the reference frame I_{ref} is assumed to be fixed. The current image I is aligned by minimization of the photometric residual $r(\xi)$ and line re-projection geometric error $g(\xi)$ corresponding to two observation model: photometric intensity observation and edge position observations. It can be formulated as the following non-linear least squares problem:

$$E(\xi) = \sum_{i \in \Omega} r_i(\xi)^T \Sigma_{r_i}^{-1} r_i(\xi) + \sum_{j \in M} g_j(\xi)^T \Sigma_{g_j}^{-1} g_j(\xi) \quad (1)$$

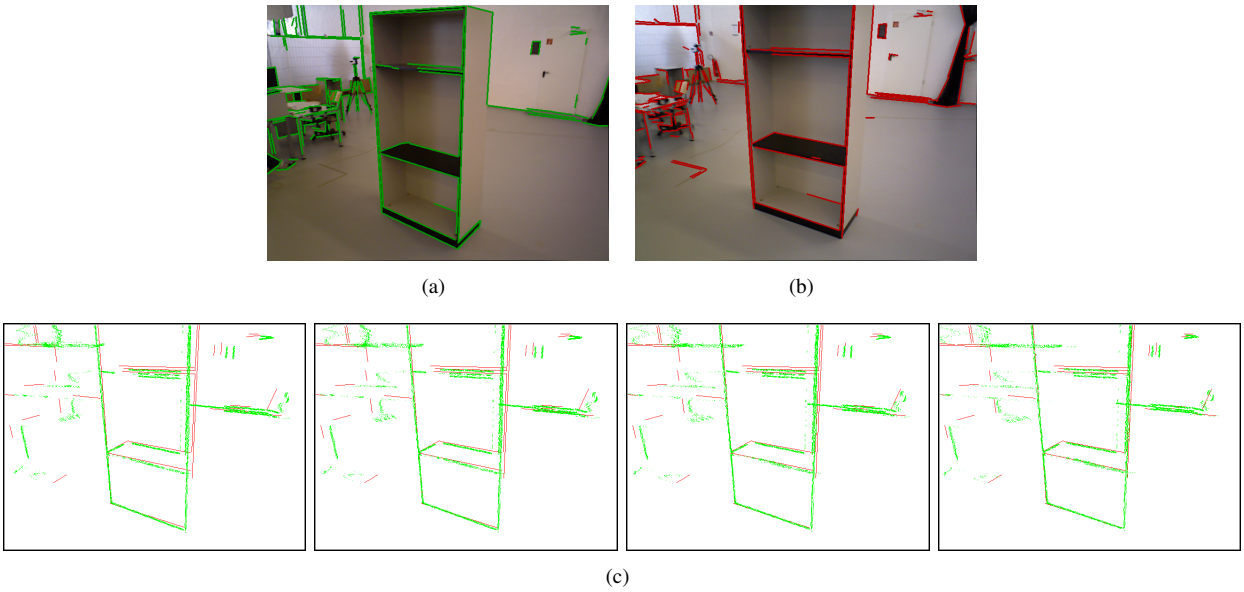

Fig. 2. Tracking iterations for two images in TUM *fr3/cabinet_big* dataset. (a) reference frame with detected edges (b) current frame with detected edges. Two frames are 41 frames apart (about 1.4s). (c) Re-projected pixels on current frame during optimization iterations corresponding to $1, 4, 9, 20$. We can see that the re-projected edge pixels in green gradually align with the true edges in red. Best viewed in color.

where photometric error r_i is defined by [6] [12]:

$$r_i = I_{ref}(x_i) - I(\tau(x_i, D_{ref}(x_i), \xi)) \tag{2}$$

g_j is the re-projection error of pixel x_i to its corresponding line l_j (homogeneous line representation):

$$g_j = l_j^T \ \widehat{\tau}(x_i, D_{ref}(x_i), \xi) \tag{3}$$

where $\widehat{\tau}()$ is the homogeneous coordinate operation. This term is only used for the pixels of edges in I_{ref} which also have a matching edge in I. Σ_r and Σ_g represents the uncertainty of two errors correspondingly.

The energy function Equation (1) is minimized through iterative Gauss-Newton optimization. For iteration n, the small update is:

$$\delta\xi^n = -(J^T W J)^{-1} J^T W \mathbf{E}(\xi^n) \tag{4}$$

Where $\mathbf{E}$ is the stacked error vectors composed of two parts: $\mathbf{E} = (r_1, ..., r_n, g_1, ..., g_m)^T$. J is the the Jacobian of $\mathbf{E}$ *wrt.* ξ. W is the weight matrix computed from uncertainty Σ^{-1}. A tracking illustration is shown in Fig 2.

B. Tracking uncertainty analysis

Combining different types of error terms in Equation (1) increases the robustness and accuracy of pose estimation. The weights of different terms are proportional to the inverse of the error variance Σ_r and Σ_g computed from the observation models. Here, we provide an analysis of Σ_g. Photometric error uncertainty Σ_r has been analysed in [6].

In the general case, the uncertainty of the output of a function $f(x)$ propagated from the input uncertainty is expressed by:

$$\Sigma_f \approx J_f \Sigma_x J_f^T \tag{5}$$

where J_f is the Jacobian of f *wrt.* x.

In our case, as defined in Equation (3), the pixel re-projection error to line is a function of line equation l_j and re-projected point $x_i' = \widehat{\tau}(x_i, D_{ref}(x_i), \xi)$. Line equation is computed by cross product of two line endpoints $l_j = p_1 \times p_2$. We can assume that the uncertainties Σ_p of end point positions p_1 and p_2 is bi-dimensional Gaussians with $\sigma = 1$. Then we can use rule in Equation (5) to compute the uncertainties of line equation coefficients l_j. It basically implies that longer line has smaller line fitting uncertainties.

We can then similarly compute the variance of re-projection point $x_i' = \widehat{\tau}(x_i, D_{ref}(x_i), \xi)$. It is a function of pixel depth $D_{ref}(x_i)$ with variance $V_{ref}(x_i)$. The final re-projection error covariance is a combination of the two uncertainty sources:

$$\Sigma_{g_j} = l_j^T \Sigma_{x_i'} l_j + x_i'^T \Sigma_{l_j} x_i' \tag{6}$$

V. Mapping

A. Overview

In the mapping thread, the depth map D_{ref} of reference frame is updated through stereo triangulation in inverse depth filtering framework [6] followed by line regularization to improve the accuracy. The camera pose is assumed to be fixed in this step. The cost function for depth optimization is defined as follows:

$$E(D) = \sum_i r_i(d)^T \Sigma_{r_i}^{-1} r_i(d) + \sum_j G_j(d)^T \Sigma_{G_j}^{-1} G_j(d) \tag{7}$$

where $r_i(d)$ is the stereo matching photometric error. SSD error over image patches is used to improve robustness. For a line l_j, we want its pixels to also form a line in 3D space after back-projection, so G_j is edge regularization cost

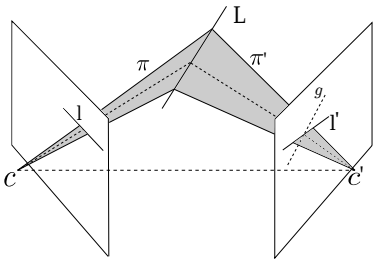

Fig. 3. Line triangulation. 3D line L could be computed by the intersection of two back-projected planes π, π'. For each pixel on l, its stereo matching point is the intersection of epipolar line g and matched edge l'. The triangulated point also lies on 3D line L. Modified from [22].

representing the distance of edge pixel's 3D point to 3D line. The regularization technique is also used in other dense mapping algorithms [12] [21]. If only the first term r_i is used [6], all the pixels are independent of each other and therefore could search independently along the epipolar line to find the matching pixel. Regularization term G_j makes the depth of pixels on one edge correlate with each other and is typically solved by an iterative alternating optimization through duality principles [12]. However, it requires much heavier computation. Instead, we optimize for r_i and G_j in two stages more efficiently.

B. Stereo match with Lines

For the pixels not on the edge or pixels on an edge which does not have a matching edge, we perform an exhaustive search for the stereo matching pixel by minimizing SSD error [6]. The depth interval for searching is limited by $d + 2\sigma_d$, where d and σ_d is the depth mean and standard deviation.

For the pixels with a matched edge, the re-projected points should lie on the matched edge as well as its epipolar line so we can directly compute their intersection as the matching point. We can also directly do line triangulation in Fig. 3 to compute all pixel's depth together. If the camera transform of current frame I wrt. I_{ref} is $R \in SO(3), \mathbf{t} \in \mathbb{R}^3$, then the 3D line L can be represented the intersection of two back-projected plane [22]:

$$L = \begin{bmatrix} \pi_1^T \\ \pi_2^T \end{bmatrix} = \begin{bmatrix} l_1^T K & 0 \\ l_2^T K R & l_2^T K \mathbf{t} \end{bmatrix} \tag{8}$$

where l_1 and l_2 are the line equation in I_{ref} and I respectively. K is the intrinsic camera parameter. Then for each pixel, we can compute the intersection of the back-projected ray with L to get its depth.

For the degenerated case where epipolar line and matched edge are (nearly) parallel, we cannot compute the 3D line accurately by plane intersection. Instead, we use the exhaustive search along the epipolar line to find the matching pixel with minimal SSD error.

C. Line matching uncertainty analysis

The uncertainty of intensity based stereo searching along epipolar line has been analysed in [6]. Here we include the analysis of edge based stereo matching error. For each edge pixel in I_{ref}, denote its epipolar line in I as g and its matched edge as l then the matching pixel is the intersection of g and l. These two lines both have positioning error ϵ_l and ϵ_g, and finally cause a disparity error ϵ_λ shown in Fig. 4. The edge uncertainty ϵ_l is already analyzed in Section IV-B which is directly related to the edge length. ϵ_λ is large when g and l are nearly parallel. Mathematically we have:

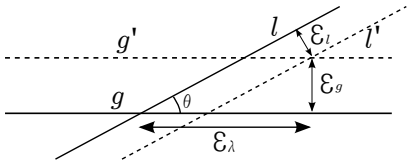

Fig. 4. Disparity error using line matching. l is the edge where the matched pixel should lie. g is the epipolar line. Due to a small positioning error ϵ_g, g is shifted to g'. The same with l' of positioning error ϵ_l. The final resulting disparity error is ϵ_λ.

$$\epsilon_\lambda = \epsilon_l / \sin(\theta) + \epsilon_g \cot(\theta) \tag{9}$$

where θ is the angle between line l and g.

From error propagation rule in Equation (5), we can compute the variance of the disparity error:

$$\sigma_\lambda^2 = \sigma_l^2 / \sin^2(\theta) + \sigma_g^2 \cot^2(\theta) \tag{10}$$

Using the approximation that inverse depth d is proportional to disparity λ, we can calculate the observation variance of d using Equation (5). It can then be used to update the pixel's depth variance in a standard EKF filtering [6].

D. 3D Line regularization

Depth map regularization is important for monocular mapping approaches to improve the depth estimation accuracy. After the depth map EKF update in Section V-C, the pixels on a 2D edge may not correspond to a line in 3D space, therefore, we need to fit lines in 3D space and update a pixel's depth. 3D weighted line fitting is recently addressed in RGB-D line based odometry [17] which utilizes Levenberg-Marquardt iterative optimization to find the best 3D line. Here we propose a fast and analytical solution to the weighted 3D line fitting problem.

Since the 3D points are back-projected from the same 2D edge, they should lie on the same plane G from projective geometry. We can create anther coordinate frame F whose x, y axis lie on the plane G. The transformed point on the new coordinate frame is denoted as p'. We first use RANSAC to select a set of inlier 2D points. The metric for RANSAC is Mahalanobis distance, which is a weighted pixel to line Euclidean distance considering the uncertainty:

$$d_{\text{mah}} = \min_{q' \in l'} (p' - q')^T \Sigma_{p'}^{-1} (p' - q') \tag{11}$$

where $q' \in l'$ indicates a point lying on line l' in frame F. d_{mah} could be computed analytically by taking the derivative *wrt.* q' and setting to zero. More details could be found in [17].

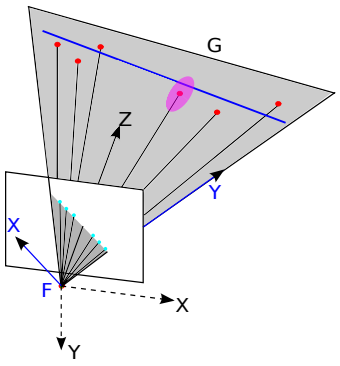

Fig. 5. 3D line regularization. We first un-project pixel to 3D shown as red dots on the 3D plane G. The pink ellipse shows the uncertainty of 3D point. We can transform 3D points to a coordinate frame F lying on the grey plane. The axis are X, Y in blue. Then we can use RANSAC to analytically compute a weighted least square line instead of iterative optimization [17]. Image modified from [17]. Best viewed in color.

After RANSAC, we can find the largest consensus set of points p'_i, $i = 1, ..., n$. This becomes a 2D weighted line fitting problem and we want to find the best line L^* so that:

$$L^* = \min_L \sum_i \delta(p'_i)^T \Sigma_{p'_i}^{-1} \delta(p'_i) \tag{12}$$

where $\delta(p'_i)$ is distance of point p'_i to line L along y axis. It is an approximation of point to line distance but could lead to a closed form solution. Stack all points p'_i coordinates as $[\mathbf{X}, \mathbf{Y}]$ (after subtracting from mean) and weight matrix as W which can be approximated as original image pixels' covariance. Then the line model under consideration is $\mathbf{Y} = \mathbf{X}\beta + \epsilon$, where β is line coefficients, and ϵ is assumed to be normally distributed vector of noise. The MLE optimal line under Gaussian noise is:

$$\widehat{\beta} = arg\min_\beta \sum_i \epsilon_i^2 = (\mathbf{X}^T W \mathbf{X})^{-1} \mathbf{X}^T W \mathbf{Y} \tag{13}$$

We can then transform the optimal line L^* in coordinate frame F back to the original camera optical frame and determine the pixel depth on the line.

VI. Experiments and Results

A. Implementation

1. Edge detection and matching: We use the public line segment detection algorithm [23]. To improve the tracking accuracy, we adopt a coarse-to-fine approach using two pyramid levels with a scale factor of two. Due to the uncertainty of line detection algorithm, one complete line can sometimes break into multiple segments so we explicitly merge two lines whose angles and distance are very close within a threshold. After that, we need to remove very short line segments which may have large line fitting error. To speed up the line merging, lines are assigned to different bucket grids indexed by the middle points of an edge and the orientation of it. Then we only need to consider possible merging within the same and nearby bucket.

We then compute the LBD descriptor [24] for each line and match them across images. Bucket technique is also utilized to speed up the matching. Finally, line tracing is performed to find all pixels on an edge. We find that the system becomes more robust and accurate if we expand the line for one pixel possibly because more pixels are involved by the line constraints in tracking and mapping.

2. Keyframe-based VO: our approach doesn't have the bundle adjustment of points and lines in SLAM and SfM framework but could be extended to improve the performance. Camera tracking, line matching and stereo mapping are implemented only between the current frame and keyframe.

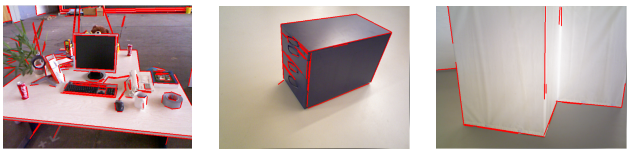

(a) (b) (c)

Fig. 6. Example images in TUM datasets with varying textures. (a) fr2/desk, (b) fr3/cabinet, (c) fr3/notex-far. ORB SLAM performs worse on (b) and (c) as there are fewer features points. Our algorithm can still utilize the matched edge features to improve the state estimation.

B. Experiments

In this section, we test our algorithm on various public datasets including TUM RGBD [25], TUM mono [26] and ICL-NUIM [27]. We mainly compare with the state of art monocular direct SDVO [6] and feature based ORB SLAM [5]. We also provide some comparison with edge based VO [18] [19] in some datasets where the result is provided. For ORB SLAM, we turn off the loop closing thread, but still keep local and global bundle adjustment (BA) to detect incremental loop-closures while our algorithm and SDVO are VO algorithm without BA. We use the relative position error metric (RPE) by Strum *et al* [25].

$$E_i = (Q_i^{-1} Q_{i+\delta})^{-1} (B_i^{-1} B_{i+\delta}) \tag{14}$$

where $Q_i \in SE(3)$ is the sequence of ground truth poses and $B_i \in SE(3)$ is the estimated pose. Scale is estimated to best align the trajectory.

1) Qualitative results: We choose TUM *mono/38* [26] for VO and mapping visualization shown in Fig. 1. It mainly contains homogeneous white surfaces but there are still many edges that could be utilized. Our method could generate good quality mapping and state estimation. More results can be found in the supplementary video.

2) Quantitative results: We first evaluate on two popular sequences of TUM RGBD dataset *fr2/desk* and *fr2/xyz* shown in Fig 6(a). Comparison is shown in Table I, where result of SDVO and two edge based VO [18] [19] are obtained from their paper. These two scenarios are feature rich environments thus are most suitable for the feature-based ORB SLAM with BA. Due to the large amounts of high gradient pixels, SDVO also performs well. Due to many curved bottles, leafs, and small keyboards, there is relatively large line detection and matching errors for these environments,

TABLE I

RELATIVE POSITION ERROR (CM/S) COMPARISON ON TUM DATASET

Sequence	Ours	SDVO	ORB-SLAM	[18]	[19]
fr2/desk	1.88	2.1	**0.7**	2.8	6.9
fr2/xyz	0.66	0.6	**0.6**	0.8	2.1

TABLE II

RELATIVE POSITION ERROR (CM/S) COMPARISON ON VARIOUS DATASETS

Sequence	Ours	SDVO	ORB-SLAM
ICL/office2	4.44	5.72	**2.11**
mono/38	2.04	5.4	**1.16**
ICL/office1	1.85	**1.33**	X
fr3/cabinet-big	**8.82**	16.23	33.57
fr3/cabinet	**13.3**	21.7	X
fr3/notex-far	**4.32**	10	X

our algorithm performs similarly to SDVO but better than two other edge based VO.

We also provide results on more datasets shown in Table II, where other edge VO doesn't provide results. The top two scenes are relative easy environments. In TUM *mono/38* in Fig. 1, we only evaluate the beginning part which has ground truth pose. Since there are still some corner points on the door and showcase, ORB-SLAM with BA still performs the best but our algorithm clearly outperforms the SDVO. This is because the door surface is nearly homogeneous without large intensity gradients so the photometric error minimization of SDVO doesn't work very well while our algorithm can still use edges to minimize edge re-projection error.

The last four scenes in Table II are more challenging feature-less environments shown in Fig .6(b) and Fig .6(c). ORB-SLAM doesn't work well and even fails (denoted as 'X') in some environments but direct VO can still work to some extent because direct methods utilize high gradient and edge pixels instead of feature points. Note that in *ICL/office1* dataset, the overall scene has many feature points but ORB SLAM failure happens when the camera only observes white walls and ground with few distinguishable features. Our method with line clearly outperforms SDVO in most of the cases from the table and there are mainly two reasons. Firstly, by adding edges, we are utilizing more pixels for tracking. Some pixels might have low gradients due to homogeneous surfaces but can still be utilized because of lying on edges shown in Fig .6(c). Secondly, we are minimizing photometric error as well as geometric error, which is known to be more robust to image noise and has a large convergence basin. This has been analysed and verified in many other works [26] [5].

To demonstrate the advantage of a large convergence basin in the optimization, we select two frames from TUM *fr3/cabinet_big* which are 41 frames apart (1.3s) and show the tracking iterations in Fig. 2. We can clearly see the re-projected pixels in green gradually align with the true edges in red.

TABLE III

TIME ANALYSSI ON TUM FR3/CABINET_BIG DATASET.

Component	Value
Edge detection	16.24 ms
Descriptor computation	11.95 ms
Edge matching	4.52 ms
Tracking time	19.23 ms
Mapping time	10.99 ms
Edge number	193

C. Time analysis

We report the time usage of our algorithm running on TUM *fr3/cabinet_big* dataset shown in Table III. Using two octaves of line detection, there are totally 193 edges on average per frame. The total tracking thread apart from mapping takes 51.95 ms, able to run around 20Hz. Time could vary depending on the amounts of pixels involved in the optimization. For now, edge detection and descriptor computation consumes most of the time. This could be speeded up using down-sampled image. Edline edge detector [28] can also be used to reduce detection time by half but it usually detects fewer edges compared to the currently used method [23] and may affect the state estimation accuracy in some challenging environments. Recently, Gomez *et al* [19] utilize edge tracking to decrease the computation instead of detection and matching for every frame, which is also a good solution.

VII. CONCLUSIONS

In this paper, we propose a direct monocular odometry algorithm utilizing points and lines. We follow the pipeline of SDVO [6] and add edges to improve both tracking and mapping performance. In the tracking part, we minimize both photometric error and geometric error to the matched edges. In the mapping part, using matched edges, we can get stereo matching quickly and accurately without exhaustive search. An analytical solution is developed to regularize the depth map using edges. We also provide probability uncertainty analysis of different observation models in tracking and mapping part.

Our algorithm combines the advantage of direct and feature based VO. It is able to create a semi-dense map and the state estimation is more robust and accurate due to the incorporation of edges and geometric error minimization. On various dataset evaluation, we achieve better or comparable performance than SDVO and ORB SLAM. ORB SLAM with bundle adjustment works the best in environments with rich features. However, for scenarios with low texture, ORB SLAM might fail and direct methods usually work better. Our algorithm focuses on these scenarios and further improves the performance of SDVO by adding edges.

In the future, we want to reduce the computation of edge detection and matching by direct edge alignment. Also, bundle adjustment of edges in multiple frames could also be used to improve the accuracy. We will also exploit more information by combining points, edges, and planes [29] in one framework to improve the accuracy and robustness in challenging environments.

ACKNOWLEDGMENTS

This work is supported by NSF award IIS-1328930.

REFERENCES

[1] Albert S Huang, Abraham Bachrach, Peter Henry, Michael Krainin, Daniel Maturana, Dieter Fox, and Nicholas Roy. Visual odometry and mapping for autonomous flight using an rgb-d camera. In *International Symposium on Robotics Research (ISRR)*, volume 2, 2011.

[2] Andreas Geiger, Julius Ziegler, and Christoph Stiller. Stereoscan: Dense 3d reconstruction in real-time. In *IEEE Intelligent Vehicles Symposium*, Baden-Baden, Germany, June 2011.

[3] Zheng Fang, Shichao Yang, Sezal Jain, Geetesh Dubey, Stephan Roth, Silvio Maeta, Stephen Nuske, Yu Zhang, and Sebastian Scherer. Robust autonomous flight in constrained and visually degraded shipboard environments. *Journal of Field Robotics*, 34(1):25–52, 2017.

[4] Georg Klein and David Murray. Parallel tracking and mapping for small ar workspaces. In *Mixed and Augmented Reality, 2007. ISMAR 2007. 6th IEEE and ACM International Symposium on*, pages 225–234. IEEE, 2007.

[5] Raul Mur-Artal, JMM Montiel, and Juan D Tardos. ORB-SLAM: a versatile and accurate monocular SLAM system. *Robotics, IEEE Transactions on*, 31(5):1147–1163, 2015.

[6] Jakob Engel, Jurgen Sturm, and Daniel Cremers. Semi-dense visual odometry for a monocular camera. In *Proceedings of the IEEE international conference on computer vision*, pages 1449–1456, 2013.

[7] Jakob Engel, Thomas Schöps, and Daniel Cremers. LSD-SLAM: Large-scale direct monocular SLAM. In *European Conference on Computer Vision (ECCV)*, pages 834–849. Springer, 2014.

[8] Rubén Gómez-Ojeda and Javier González-Jiménez. Robust stereo visual odometry through a probabilistic combination of points and line segments. 2016.

[9] Manohar Prakash Kuse and Shaojie Shen. Robust camera motion estimation using direct edge alignment and sub-gradient method. In *IEEE International Conference on Robotics and Automation (ICRA), Stockholm, Sweden*, 2016.

[10] Jakob Engel, Vladlen Koltun, and Daniel Cremers. Direct sparse odometry. *arXiv preprint arXiv:1607.02565*, 2016.

[11] Raúl Mur-Artal and Juan D Tardós. Probabilistic semi-dense mapping from highly accurate feature-based monocular SLAM. *Proceedings of Robotics: Science and Systems, Rome, Italy*, 2015.

[12] Richard A Newcombe, Steven J Lovegrove, and Andrew J Davison. Dtam: Dense tracking and mapping in real-time. In *2011 international conference on computer vision*, pages 2320–2327. IEEE, 2011.

[13] Christian Kerl, Jürgen Sturm, and Daniel Cremers. Dense visual slam for rgb-d cameras. In *2013 IEEE/RSJ International Conference on Intelligent Robots and Systems*, pages 2100–2106. IEEE, 2013.

[14] Ethan Eade and Tom Drummond. Edge landmarks in monocular slam. *Image and Vision Computing*, 27(5):588–596, 2009.

[15] Georg Klein and David Murray. Improving the agility of keyframe-based slam. In *European Conference on Computer Vision*, pages 802–815. Springer, 2008.

[16] Jonas Witt and Uwe Weltin. Robust stereo visual odometry using iterative closest multiple lines. In *2013 IEEE/RSJ International Conference on Intelligent Robots and Systems*, pages 4164–4171. IEEE, 2013.

[17] Yan Lu and Dezhen Song. Robust rgb-d odometry using point and line features. In *Proceedings of the IEEE International Conference on Computer Vision*, pages 3934–3942, 2015.

[18] Juan Jose Tarrio and Sol Pedre. Realtime edge-based visual odometry for a monocular camera. In *Proceedings of the IEEE International Conference on Computer Vision*, pages 702–710, 2015.

[19] Ruben Gomez-Ojeda, Jesus Briales, and Javier Gonzalez-Jimenez. Plsvo: Semi-direct monocular visual odometry by combining points and line segments. In *Intelligent Robots and Systems (IROS), 2016 IEEE/RSJ International Conference on*, pages 4211–4216. IEEE, 2016.

[20] Richard M Murray, Zexiang Li, S Shankar Sastry, and S Shankara Sastry. *A mathematical introduction to robotic manipulation*. CRC press, 1994.

[21] Pedro Piniés, Lina Maria Paz, and Paul Newman. Dense mono reconstruction: Living with the pain of the plain plane. In *2015 IEEE International Conference on Robotics and Automation (ICRA)*, pages 5226–5231. IEEE, 2015.

[22] Richard Hartley and Andrew Zisserman. *Multiple view geometry in computer vision*. Cambridge university press, 2003.

[23] von Gioi R Grompone, Jeremie Jakubowicz, Jean-Michel Morel, and Gregory Randall. Lsd: a fast line segment detector with a false detection control. *IEEE transactions on pattern analysis and machine intelligence*, 32(4):722–732, 2010.

[24] Lilian Zhang and Reinhard Koch. An efficient and robust line segment matching approach based on lbd descriptor and pairwise geometric consistency. *Journal of Visual Communication and Image Representation*, 24(7):794–805, 2013.

[25] Jürgen Sturm, Nikolas Engelhard, Felix Endres, Wolfram Burgard, and Daniel Cremers. A benchmark for the evaluation of RGB-D SLAM systems. In *Intelligent Robots and Systems (IROS), IEEE/RSJ International Conference on*, pages 573–580. IEEE, 2012.

[26] J. Engel, V. Usenko, and D. Cremers. A photometrically calibrated benchmark for monocular visual odometry. In *arXiv:1607.02555*, July 2016.

[27] A. Handa, T. Whelan, J.B. McDonald, and A.J. Davison. A benchmark for RGB-D visual odometry, 3D reconstruction and SLAM. In *IEEE Intl. Conf. on Robotics and Automation, ICRA*, Hong Kong, China, May 2014.

[28] Cuneyt Akinlar and Cihan Topal. Edlines: A real-time line segment detector with a false detection control. *Pattern Recognition Letters*, 32(13):1633–1642, 2011.

[29] Shichao Yang, Yu Song, Michael Kaess, and Sebastian Scherer. Pop-up SLAM: a semantic monocular plane slam for low-texture environments. In *Intelligent Robots and Systems (IROS), 2016 IEEE international conference on*. IEEE, 2016.